



ELSEVIER

Available online at www.sciencedirect.com

SCIENCE @ DIRECT®

Physica E 28 (2005) 374–384

PHYSICA E

www.elsevier.com/locate/physce

Localized electronic states in N -layer-based superlattices with structural defects

Wei-Qing Huang^{a,b}, Ke-Qiu Chen^{a,b,*}, Z. Shuai^{b,*}, Lingling Wang^a,
Wangyu Hu^a, B.S. Zuo^a

^aDepartment of Applied Physics, Hunan University, Changsha 410082, China

^bLaboratory of Organic Solids, Center for Molecular Sciences, Institute of Chemistry, Chinese Academy of Sciences, 100080 Beijing, PR China

Received 4 April 2005; accepted 14 April 2005

Available online 11 July 2005

Abstract

Using an effect-barrier height method, we study the properties of the localized electronic states in an N -layer-based superlattice with structural defects within the framework of effective-mass theory. The coupling effect between normal and lateral degrees of freedom of an electron on the localized electronic states in both symmetric and asymmetric triple layer superlattices with structural defects has been considered numerically. The results show that the localized states display different behaviors in both symmetric and asymmetric structures in spite of the minibands being not influenced by the structural symmetry. Moreover, the coupling effect causes the minibands, minigaps and localized electron levels to depend on the transverse wave number k_{xy} . A brief physical analysis is given.

© 2005 Elsevier B.V. All rights reserved.

PACS: 73.21.-b; 71.23.An; 73.21.Cd

Keywords: Electron states; Localized states; Superlattices

1. Introduction

In recent years, superlattices (SLs) in the presence of inhomogeneities such as surface, interface or

defect layer have attracted much attention due to novel physical properties found in this type of structure in comparison with ideal SLs. It is known that the introduction of the defect layer in SLs can lead to the localization of electronic states [1–11], acoustic modes [12–17], optical modes [18–20] and interface plasmon modes [21,22] in the vicinity of the defects. As far as electronic states in this type of structure are concerned, deviation of the structure from strict periodicity should result in the creation

*Corresponding author. Department of Applied Physics, Hunan University, Changsha 410082, China.
Tel.: +86 0731 8820375; fax: +86 0731 8822332.

E-mail addresses: keqiuchen@iccas.ac.cn, keqiuchen@hnu.cn (K.-Q. Chen), zgshuai@iccas.ac.cn (Z. Shuai).

of localized states within the minigaps. The properties of localized electronic states in a semi-infinite SL [1,3–6,8,9] and infinite SL with structural defects [2,7,10,11] have been reported. However, many previous works based on the effective-mass parabolic conduction-band model paid little attention to the coupling effect between normal and lateral degrees of freedom of an electron and assumed that the energy of an electron may be separated into longitudinal and transverse components in the whole structure, irrespective of the effective mass mismatches in different constituent layers. Some studies have shown that the mismatch of electron effective mass in different constituent layers can lead to significant dependence of the electron levels on the transverse wave number k_{xy} in quantum wells and SLs [23–25].

Recently, Chen et al. studied the localized electronic states in a binary SL with a structural defect layer and showed that miniband, minigap and localized levels are obviously dependent on the transverse wave vector k_{xy} in an infinite binary SL with a structural defect layer [26]. More recently, Huang et al. investigated the surface electronic states in a semi-infinite SL with a cap layer [27]. The results also stated that the coupling effect should be considered when the difference of the electron effective mass between well and barrier materials cannot be neglected.

The present work extends these studies to a general infinite N -layer-based SL with structural defects. We derive general formulae for calculating localized and extended electronic states in such a system by using the transfer-matrix method. In comparison, the localized electronic states in both symmetric and asymmetric SL structures with the structural defects are discussed.

In the next section, a brief description of the theoretical framework of our calculation is presented. The numerical results will be introduced in Section 3 with analyses, and a brief summarization will form the last section.

2. Model and formalism

We consider two typical samples of the SLs with structural defects: (i) symmetric structure, in which a

defect region labelled as d is embedded between two semi-infinite SLs, each of them is formed by an infinite repetition of a unit cell containing N different slabs with thicknesses L_{av} , potential heights U_{av} and effective masses m_{av} ($v = 1, 2, \dots, N$), and the defect region is composed of s slabs with thicknesses $L_{d\kappa}$, potential heights $U_{d\kappa}$ and effective masses $m_{d\kappa}$ ($\kappa = 1, 2, \dots, s$), as depicted in Fig. 1(a); (ii) asymmetric structure, formed by inserting a defect region consisted of s slabs into an infinite SL, depicted in Fig. 1(b). The period of the SL is $L = L_{a1} + L_{a2} + \dots + L_{aN}$. We choose the growth direction of the SLs as the z axis and the center of the structural defects as the coordinate origin.

Within the envelope function effective-mass approximation, the electron 1D Schrödinger equation satisfied by the longitudinal envelope-wave function $\phi(z)$ is described by

$$-\frac{\hbar^2}{2} \frac{d}{dz} \frac{1}{m(z)} \frac{d}{dz} \phi(z) + U(z)\phi(z) = \left[E - \frac{\hbar^2 k_{xy}^2}{2m(z)} \right] \phi(z), \quad (1)$$

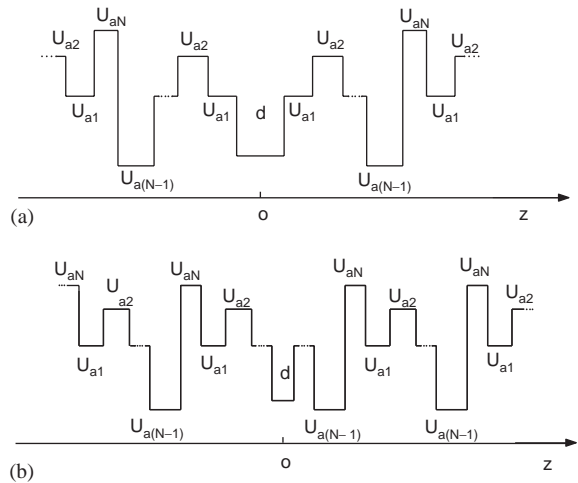


Fig. 1. (a) Symmetric structure: schematic diagram of two semi-infinite SLs with an embedded structural defect d . (b) asymmetric structure: schematic diagram of an infinite SL with structural defect d inserting into a cell. U_{a1}, U_{a2}, \dots , and U_{aN} represent the potential barrier heights of the corresponding constituent av layer in one cell, respectively. U_d denotes the conduction band edge of the defect layer.

where k_{xy} is the transverse wave number, and $U(z)$ and $m(z)$ are the position-dependent potential and the effective mass, respectively. From Eq. (1), we have $E_z^i = E - E_{xy}^i$ representing the longitudinal energies of the electron in the i th layer, where $E_{xy}^i = \hbar^2 k_{xy}^2 / 2m_i$ is the transverse kinetic energies in the i th layer. Taking into account the difference of the effective mass of the electron in different layers in a cell, i.e. $m_i \neq m_j$, both the transverse kinetic energy and longitudinal energy components of the electron no longer keep their conservation individually. We introduce an effective barrier height $U_{\alpha i}(k_{xy})$ ($\alpha = a, d$, $i = v, \kappa$) of the i th layer [26,27]:

$$U_{\alpha i}(k_{xy}) = U_{\alpha i} - \left(1 - \frac{m_{\alpha t}}{m_{\alpha i}}\right) \frac{\hbar^2 k_{xy}^2}{2m_{\alpha t}}, \quad (2)$$

where $U_{\alpha i}$ is the potential of the i th layer. Without any loss of generality, we assume that the potential of the t th layer in a cell is zero.

Eq. (1) can then be rewritten as

$$-\frac{\hbar^2}{2} \frac{d}{dz} \frac{1}{m(z)} \frac{d}{dz} \phi(z) + U_{\text{eff}}(z) \phi(z) = E_z \phi(z), \quad (3)$$

where $E_z \equiv E_z^t = E - (\hbar^2 k_{xy}^2 / 2m_{\alpha t})$, and the effective potential $U_{\text{eff}}(z)$ is defined as follows:

$$U_{\text{eff}}(z) = \begin{cases} 0 & \text{in the } t\text{th layer,} \\ U_{\alpha i}(k_{xy}) & \text{in the } i\text{th layer.} \end{cases} \quad (4)$$

From Eq. (4), it is evident that the longitudinal component of the motion of the electron is dependent on the transverse wave vector k_{xy} when taking into account the difference of the effective mass of the electron in the different layers.

The above equations are applied to investigate localized electron levels in the structures as shown in Fig. 1. At the v th layer in a cell, the longitudinal envelope-wave function can be written as

$$\phi(n, v, z) = [A_{\alpha v} e^{ik_{\alpha v}(z-z_{\alpha v}^n)} + B_{\alpha v} e^{-ik_{\alpha v}(z-z_{\alpha v}^n)}] e^{iq_z(n-1)L}. \quad (5)$$

In the defect region,

$$\phi(d, \kappa, z) = A_{d\kappa} e^{ik_{d\kappa}(z-z_{d\kappa})} + B_{d\kappa} e^{-ik_{d\kappa}(z-z_{d\kappa})}, \quad (6)$$

where $z_{d\kappa}$ represents the center coordinate of the κ th slab in the defect region, $z_{\alpha v}^n$ is the center

coordinate of the v th layer in the n th ($n = 1, 2, \dots, N$) period of the SL, L is the period of the SL, and the longitudinal wave number of the electron k_{zi} in the i th layer is given by

$$k_{zi} = \left[\frac{2m_{\alpha i}(E_z - U_{\text{eff}})}{\hbar^2} \right]^{1/2}. \quad (7)$$

For localized electronic states lying within minigaps, the Bloch wave number q_z should take complex values in the form of

$$q_z = \frac{n\pi}{L} + iq \quad (q \geq 0, n = 0, 1, 2, \dots), \quad (8)$$

where n denotes the index of minigaps. It should be noted that the imaginary Bloch wave number q (decay factor) describes the localization degree of the localized modes in the vicinity of the defect layer.

Bastard's boundary conditions applied to the SL interfaces— $\phi(z)$ and $\phi'(z)/m(z)$ —should be continuous at each interface; the following equations are obtained:

$$\cos(q_z L) - 0.5(\hat{P}_{11} + \hat{P}_{22}) = 0, \quad (9)$$

$$\begin{aligned} &(\hat{G}_{11} + C\hat{G}_{12})(\hat{H}_{21} + C'\hat{H}_{22}) \\ & - (\hat{G}_{21} + C\hat{G}_{22})(\hat{H}_{11} + C'\hat{H}_{12}) = 0, \end{aligned} \quad (10)$$

where

$$C = (e^{-iq_z L} - \hat{P}_{11}) / \hat{P}_{12}, \quad (11)$$

$$C' = (e^{-iq_z L} - \hat{P}'_{11}) / \hat{P}'_{12}, \quad (12)$$

$$\begin{aligned} \hat{G} &= \hat{T}^{-1}(m_{d1}, k_{d1}, L_{d1}) \prod_{r=2}^S \hat{M}(m_{dr}, k_{dr}, L_{dr}) \\ &\times \hat{T}(m_{\alpha 1}, k_{\alpha 1}, -L_{\alpha 1}), \end{aligned} \quad (13)$$

$$\begin{aligned} \hat{P} &= \hat{T}^{-1}(m_{n,\alpha v}, k_{n,\alpha v}, L_{n,\alpha v}) \\ &\times \prod_{p=v+1}^N \hat{M}(m_{n,\alpha p}, k_{n,\alpha p}, L_{n,\alpha p}) \\ &\times \prod_{r=1}^{v-1} \hat{M}(m_{n+1,\alpha r}, k_{n+1,\alpha r}, L_{n+1,\alpha r}) \\ &\times \hat{T}(m_{n+1,\alpha r}, k_{n+1,\alpha r}, -L_{n+1,\alpha r}), \end{aligned} \quad (14)$$

$$\hat{P}' = \begin{cases} \hat{T}^{-1}(m_{a1}, k_{a1}, -L_{a1}) \prod_{r=2}^N \hat{M}'(m_{ar}, k_{ar}, L_{ar}) \\ \quad \times \hat{T}(m_{a1}, k_{a1}, L_{a1}) & \text{(symmetric structure),} \\ \hat{T}^{-1}(m_{aN}, k_{aN}, -L_{aN}) \prod_{r=1}^{N-1} \hat{M}'(m_{a(N-r)}, k_{a(N-r)}, L_{a(N-r)}) \\ \quad \times \hat{T}(m_{aN}, k_{aN}, L_{aN}) & \text{(asymmetric structure),} \end{cases} \quad (15)$$

$$\hat{H} = \begin{cases} \hat{T}^{-1}(m_{d1}, k_{d1}, L_{d1}) \hat{T}(m_{a1}, k_{a1}, -L_{a1}) & \text{(symmetric structure),} \\ \hat{T}^{-1}(m_{d1}, k_{d1}, L_{d1}) \hat{T}(m_{aN}, k_{aN}, -L_{aN}) & \text{(asymmetric structure)} \end{cases} \quad (16)$$

with

$$\hat{M}(m, k, z) = \hat{T}(m, k, -z) \hat{T}^{-1}(m, k, z), \quad (17)$$

$$\hat{M}'(m, k, z) = \hat{T}(m, k, z) \hat{T}^{-1}(m, k, -z), \quad (18)$$

$$\hat{T}(m, k, z) = \begin{pmatrix} e^{ikz/2} & e^{-ikz/2} \\ (ik/m)e^{ikz/2} & (-ik/m)e^{-ikz/2} \end{pmatrix}. \quad (19)$$

Eqs. (7)–(10) determine the localized electron states lying within the minigaps. For real Bloch wave number q_z , Eqs. (7) and (9) give the dispersion relation of the electron states in SL.

3. Numerical results and discussion

For numerical calculations, the $\text{Al}_x\text{Ga}_{1-x}\text{As}$ -based SL has been considered, as it allowed us to realize and manipulate a wide range of potential profiles. More specifically, the potential height and the effective-mass value of a particular $\text{Al}_x\text{Ga}_{1-x}\text{As}$ layer can be adjusted by the Al concentration x , e.g., according to the empirical relations $U(x) = 944x \text{ meV}$ and $m(x) = (0.067 + 0.083x) m_e$, m_e being the free-electron mass [4]. For numerical simplicity, we consider a three-layer-based SL, where each cell consists of $a1, a2$ and $a3$ layers. The values of x in $a1, a2$ and $a3$ layers are 0.4, 0 and 0.1, respectively. The defect region consists of only one layer made of GaAs (i.e., $x = 0$).

To envisage the coupling effect between normal and lateral degrees of freedom of an electron, we

begin with the study of the influence of the transverse wave number k_{xy} on the longitudinal energy components of the localized states in the structures shown in Fig. 1. The calculated electronic structures are shown in Figs. 2(a) and (b) for symmetric and asymmetric structures, respectively. The lower and higher shade regions are denoted as minibands 1 and 2, and the three regions from low to high separated by the two allowed minibands represent the zeroth, first and second minigaps, respectively. Here, note that the zeroth and second minigaps lie at the reduced mini-Brillouin zone center, and the first minigap at the zone edge. The solid curves $a1$ – $a3$, $a20$ – $a30$, and $b1$ – $b5$ represent the longitudinal energy spectra of the localized states lying in the corresponding minigaps. For symmetric structure, it is clearly seen from Fig. 2(a) that only one localized state exists in each minigap and merges into the bulk band when the transverse wave number k_{xy} reaches a certain value. A new localized state appears at bigger k_{xy} after the first one merges into the bulk band in the first and second minigaps, respectively. By calculations, we find that the localized states possess definite parity, and the parity of $a2$ and $a30$ is odd, while the parity of $a1$, $a20$ and $a3$ is even. For asymmetric structure, one localized state appears at the zeroth minigap, and two states exist in the first and second minigaps, respectively (Fig. 2(b)). When $k_{xy} > 6.3\pi/L$ and $k_{xy} > 5.3\pi/L$, the higher localized state in the first and second minigaps merges into the second and third minibands, respectively. The different behaviors of the localized states for the different types of structures can be well understood. As is well known, the formation of the minibands originates from the

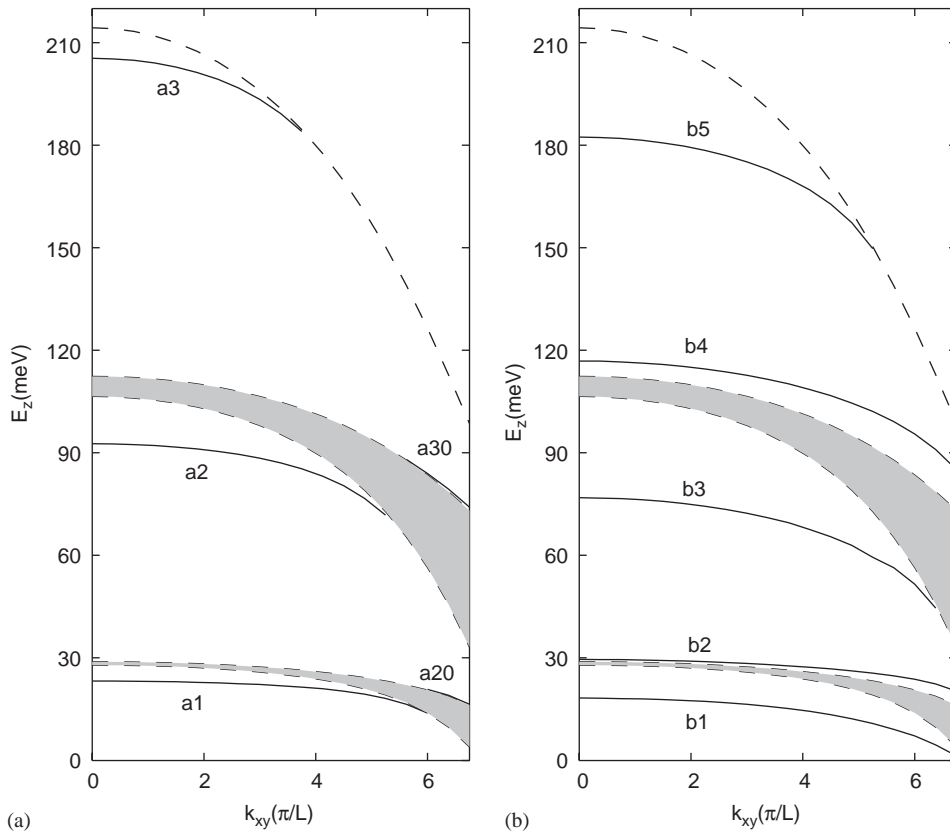


Fig. 2. Dependence of localized electronic levels on the transverse wave number k_{xy} : (a) for symmetric structure, (b) for asymmetric structure. Here $L_{a1} = 3.0$ nm, $L_{a2} = 10.0$ nm, $L_{a3} = 3.0$ nm, and $L_d = 12.5$ nm. The three regions from low to high separated by two minibands represent the zeroth, first and second minigaps, respectively. The dashed lines describe the boundary of minibands and minigaps. The solid curves represent the localized energy spectra lying in minigaps.

splitting of levels due to the periodicity coupling between the adjacent quantum wells for a perfect SL. As expected, we can find from Fig. 2 that the minibands are same for both the symmetric and asymmetric structures since it has nothing to do with the stack sequence of the constituent layers in an ideal triple-constituent SL. When introducing structural defects into a perfect SL, the periodicity coupling is locally broken down around the structural defects. The periodicity-broken coupling occurs, and leads to the appearance of new splitting levels, where some of them are localized states residing in the minigaps, while others turn into the delocalized scattering states lying in the minibands. For the symmetric structure considered here, the potential barriers at both sides of the defect layer (i.e., a quantum well) are same. For

asymmetric structure, however, the two potential barriers are different from each other. So the coupling strengths between the defect layer and its two adjacent quantum wells are different for symmetric and asymmetric structures, which results in the different behaviors of the localized states in the two structures. From Fig. 2, we can also find that all minibands, minigaps and localized energy levels always monotonically shift towards the lower energy region with the increase of the transverse wave number k_{xy} . Besides, on increasing the transverse wave number k_{xy} the width of the minigap becomes narrower, while an opposite behavior for the miniband is observed. Also the change of the higher-lying minibands and minigaps is faster than that of the lower ones, indicating that the higher-lying minibands and

minigaps are more sensitive to the variation of the k_{xy} . These results are attributed to the decrease of the effective-barrier height caused by the coupling effect as the transverse wave number k_{xy} increases (see Eq. (2)).

To clearly reveal the effect of the defect layer on the localized states in both symmetric and asymmetric structures, we display the influence of the defect layer thickness L_d on the longitudinal energy components of the localized states, as shown in Figs. 3(a) (symmetric structure) and (b) (asymmetric structure). From Fig. 3, it can be found that with the increase of the thickness L_d , the localized states appear periodically in each minigap, and the branch number of the localized states increases with the index of the minigap for a given range of the thickness L_d . As far as each

branch of the localized state is concerned, its level always shifts from the higher miniband edge to the lower one across the minigap. Moreover, it looks like the localized levels lying in the lower minigap are the elongations of corresponding levels lying in the higher minigaps, except for the first localized state in each minigap for asymmetric structure. This clearly indicates the evolution of the localized states inside the minigaps.

As is well known, each eigenstate in the confined systems with space-reverse symmetry has a definite parity, i.e., the parity of the wave function of the electronic states must be either even or odd as long as the eigenstate is nondegenerate. In order to elucidate the parity of the localized states, the wave functions of localized states in the second minigap for different L_d are shown in Fig. 4

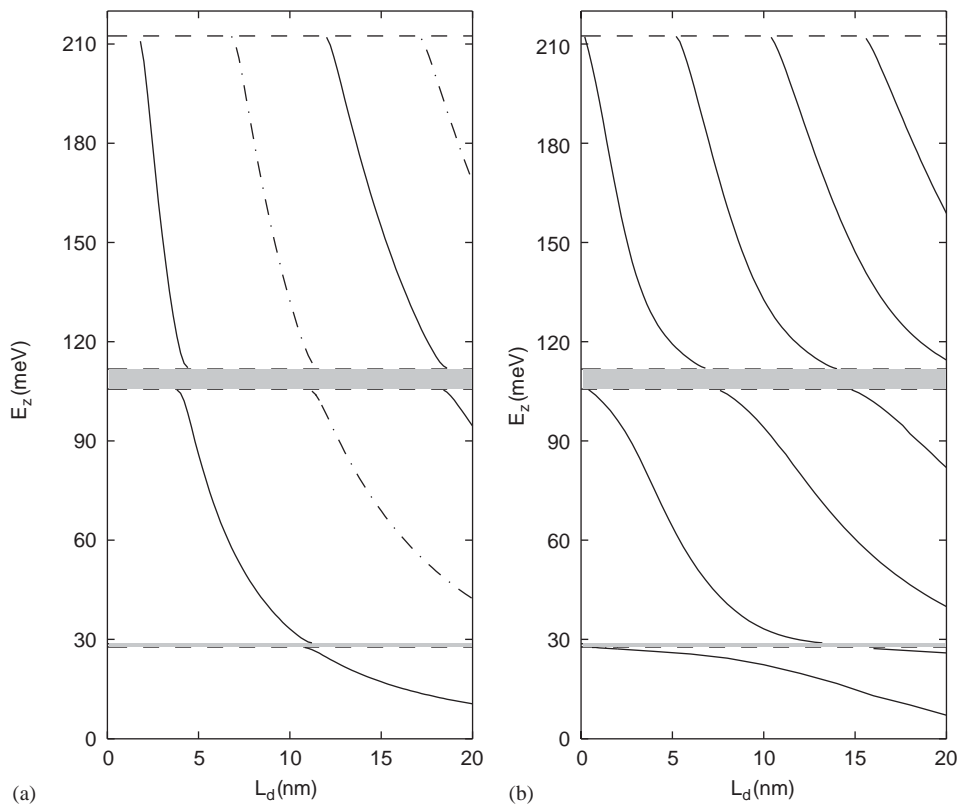


Fig. 3. Dependence of the localized levels on the defect layer thickness L_d of SLs : (a) for symmetric structure, (b) for asymmetric structure. The solid and dash-dot curves represent the localized energy spectra lying in minigaps. Here, $L_{a1} = 3.0$ nm, $L_{a2} = 10.0$ nm, $L_{a3} = 3.0$ nm, and $k_{xy} = 1.0\pi/L$. Others are the same as in Fig. 2.

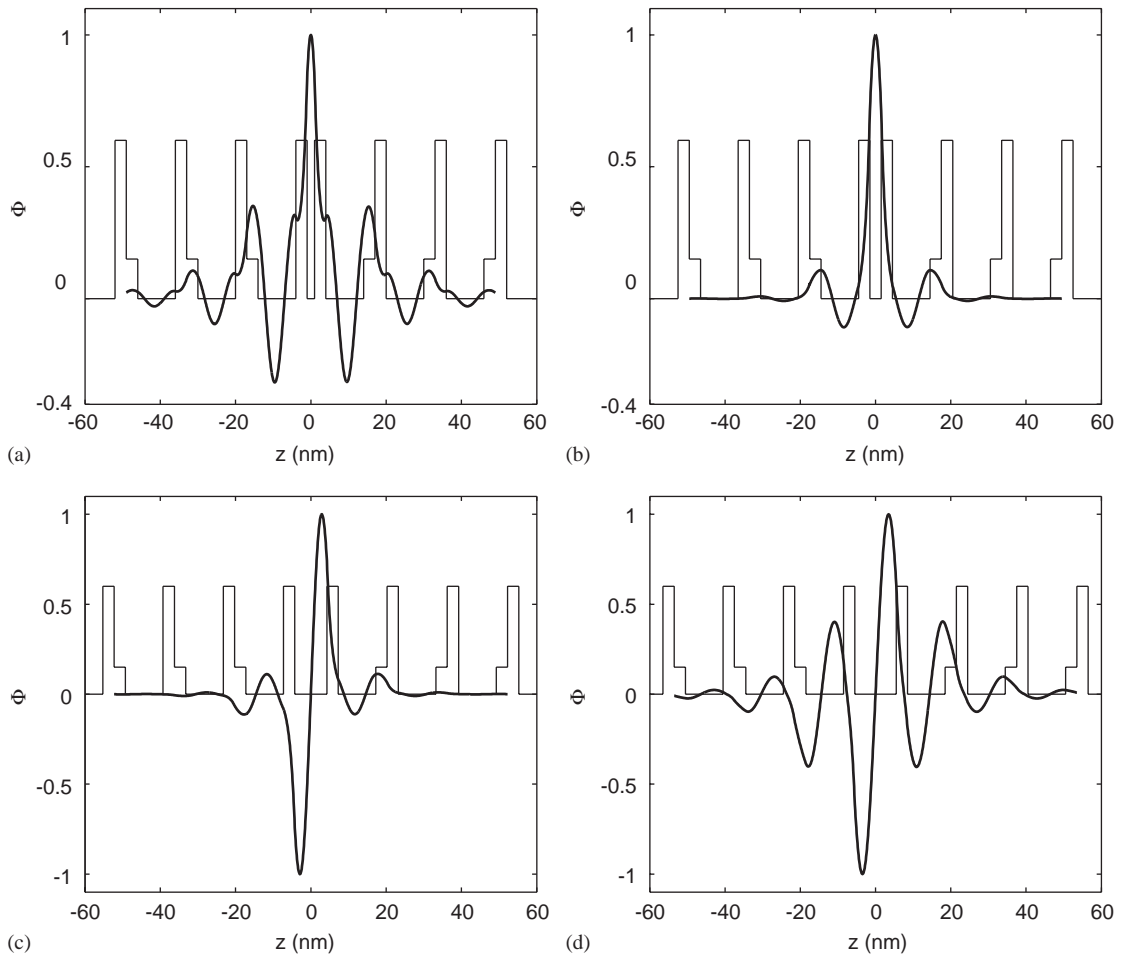


Fig. 4. The wave function ϕ (normalized to reach a maximum value of 1) of localized states in the second minigap in Fig. 2(a) for different defect layer thicknesses: (a) $L_d = 2.0$ nm, (b) $L_d = 3.0$ nm, (c) $L_d = 8.5$ nm and (d) $L_d = 11.0$ nm.

for symmetric structure: Figs. 4(a), (b), (c) and (d) correspond to $L_d = 2.0, 3.0, 8.5$ and 11.0 nm in Fig. 3(a), respectively. It is clearly observed from Fig. 4 that the parities of the localization branches (a), (b) are even, and (c) and (d) odd. Similar phenomena are found in the first minigap. Thus, we can conclude that the parity of the localized states alternates between even and odd parity with the increasing of L_d . By comparing Fig. 4(a) with (b), (c) and (d), it is clear that the localization degree of the localized electron state becomes stronger when the localized state moves from the band edge to the center of the minigap, similar to

those of localized acoustic modes and optical modes [13,18].

The wave functions of localized states in second minigaps for asymmetric structure are also shown in Fig. 5: Figs. 5(a) and (b) correspond to $L_d = 8.5$ and 13.0 nm in Fig. 3(b), respectively. As expected, one can clearly observe that the wave function of the localized state has no definite parity in such an asymmetric structure. Moreover, the wave function is mostly localized at the left side of the defect layer. This is due to the fact that for the asymmetric structure shown in Fig. 1(b), the potential barrier of the left side of the defect layer

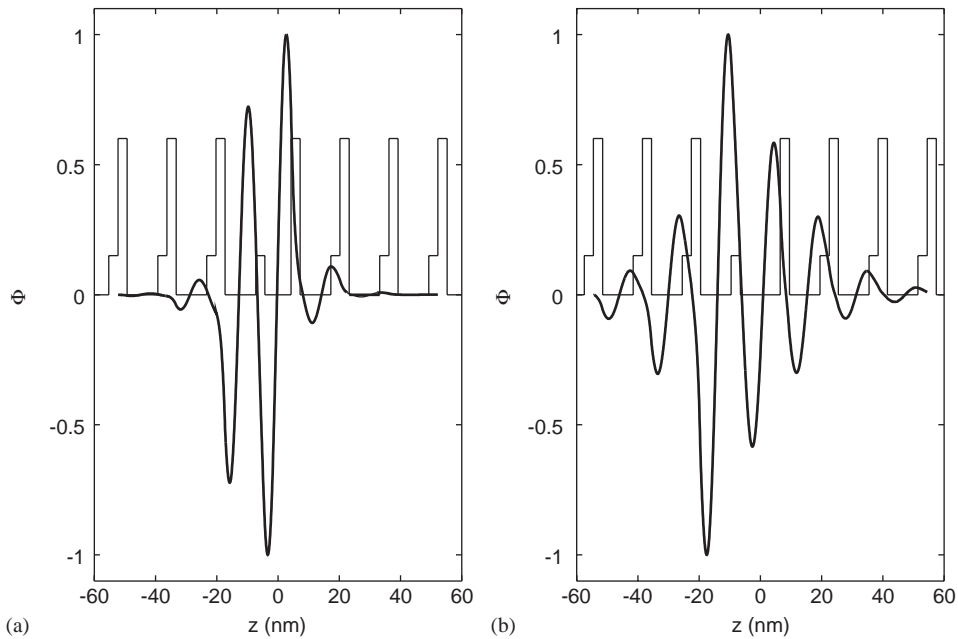


Fig. 5. The wave function ϕ (normalized to reach a maximum value of 1) of localized states in the second minigap in Fig. 2(b) for different defect layer thicknesses: (a) $L_d = 8.5$ nm, (b) $L_d = 13.0$ nm.

is lower than that of the other side. As a result, the electron wave function is easier to damp towards the region with the lower potential barrier.

We now envisage the influence of the potential height of the defect layer, the variations of the localized energy levels with U_d for both symmetric and asymmetric structures are presented in Figs. 6(a) and (b), respectively. Fig. 6(a) shows that the localized sub-level shifts almost linearly towards the high-energy region from the lower miniband to the higher one as defect layer potential height U_d increases for symmetric structure. By calculation, we know that for given structural parameters there are no localized states appearing in the zeroth minigap for $U_d > 30$ meV, in the first minigap for $U_d > 85$ meV, and in the second minigap for $U_d > 200$ meV. However, for an asymmetric structure, as shown in Fig. 6(b), the localized sub-level extends towards the bigger potential height U_d .

Figs. 7(a1)–(a3) and (b1)–(b3) describe the influence of variation of different layer thicknesses of the SL on the localized electron states in both

symmetric and asymmetric structures, respectively. As can be seen in Fig. 7, increasing the thicknesses of constituent layers causes a significant narrowing of the miniband. However, the behavior of the miniband versus the thickness of the constituent layer is different for the different varied constituent layer. Such a behavior has been explained in terms of a simple potential-profile-picture by Kucharczyk et al. [9]. Our interest focuses on the effect of the constituent layers on the localized electron states. From Figs. 7(a1) and (b1), we can find that with the increase of the thickness of layer a_1 , all the localized levels in both symmetric and asymmetric structures change rapidly for the scope $L_{a1} < 3$ nm, and then remain almost unchanged. The lower localized state in the first and second minigaps in symmetry structure merges into the first and second minibands and ceases to exist at $L_{a1} \simeq 2$ nm, respectively, while it exists in the whole explored range in the asymmetry structure. The localized states in asymmetry structure are closer to the center of the minigap in each minigap than those in symmetry structure when $L_{a1} > 3$ nm,

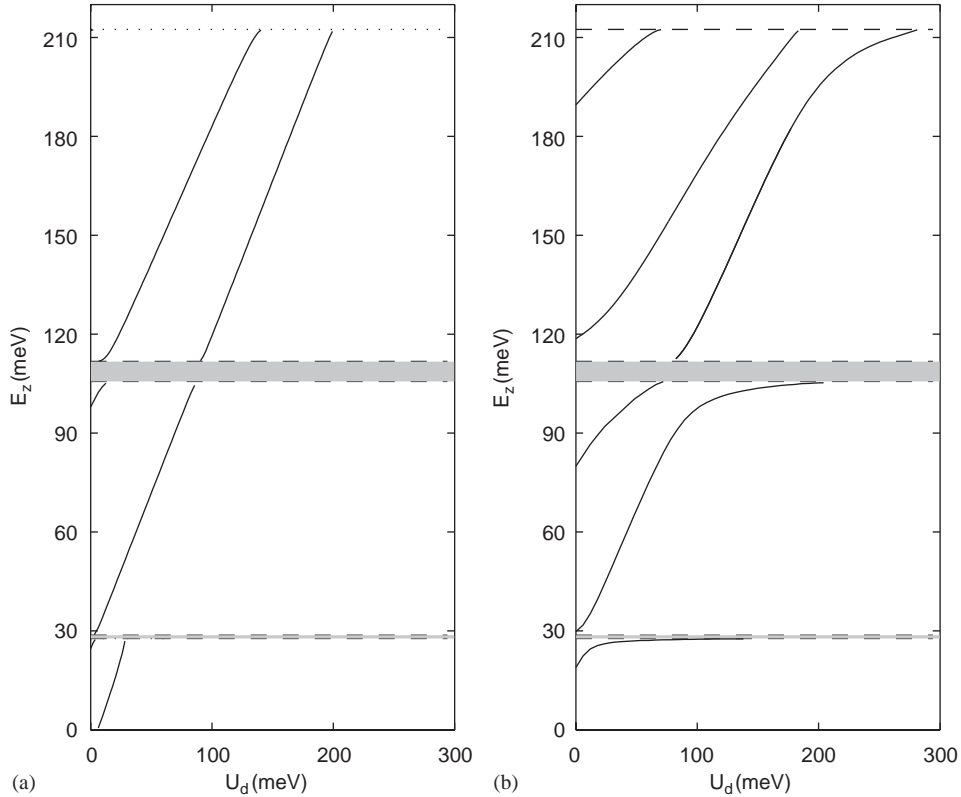


Fig. 6. Localized levels dependence on the potential height of the defect layer: (a) for symmetric structure, (b) for asymmetric structure. Here $L_d = 12.0$ nm. Others are the same as those in Fig. 2.

which shows that the localization degree of the electron states in the vicinity of the defect layer is stronger in asymmetric structure than in symmetric structure. When increasing L_{a2} , the localized states rapidly shift towards lower energy in asymmetric structure, while for the localized states in symmetric structure only a small shift-down in energy is found [see Figs. 7(a2) and (b2)]. From Fig. 7(a3), it is clear that the localized levels in the symmetric structure are not sensitive to the thickness of the layer $a3$. However, from Fig. 7(b3), we find that the localized levels change obviously with the thickness of the layer $a3$ except that the upper localization branch in the first minigap remains almost unchanged. From these results, we can conclude that the localized states in symmetric structure are more sensitive to the first constituent layer than to the other constituent layers in a certain thickness scope, which indicates

that localized states are predominantly governed by the coupling between the defect layer and its nearest constituent layer. For the asymmetric structure, however, the localized states are sensitive to all the constituent layers, especially to the constituent layer with the lowest potential. From these results, we can obtain rich localized electronic spectra by adjusting the parameters of the presented microstructures, and structural symmetry.

4. Summary

In this paper, we derive general formulae to calculate the localized electronic states considering the effect of coupling between the electronic transverse and longitudinal motion in an infinite N -layered-based SL with structural defects. In

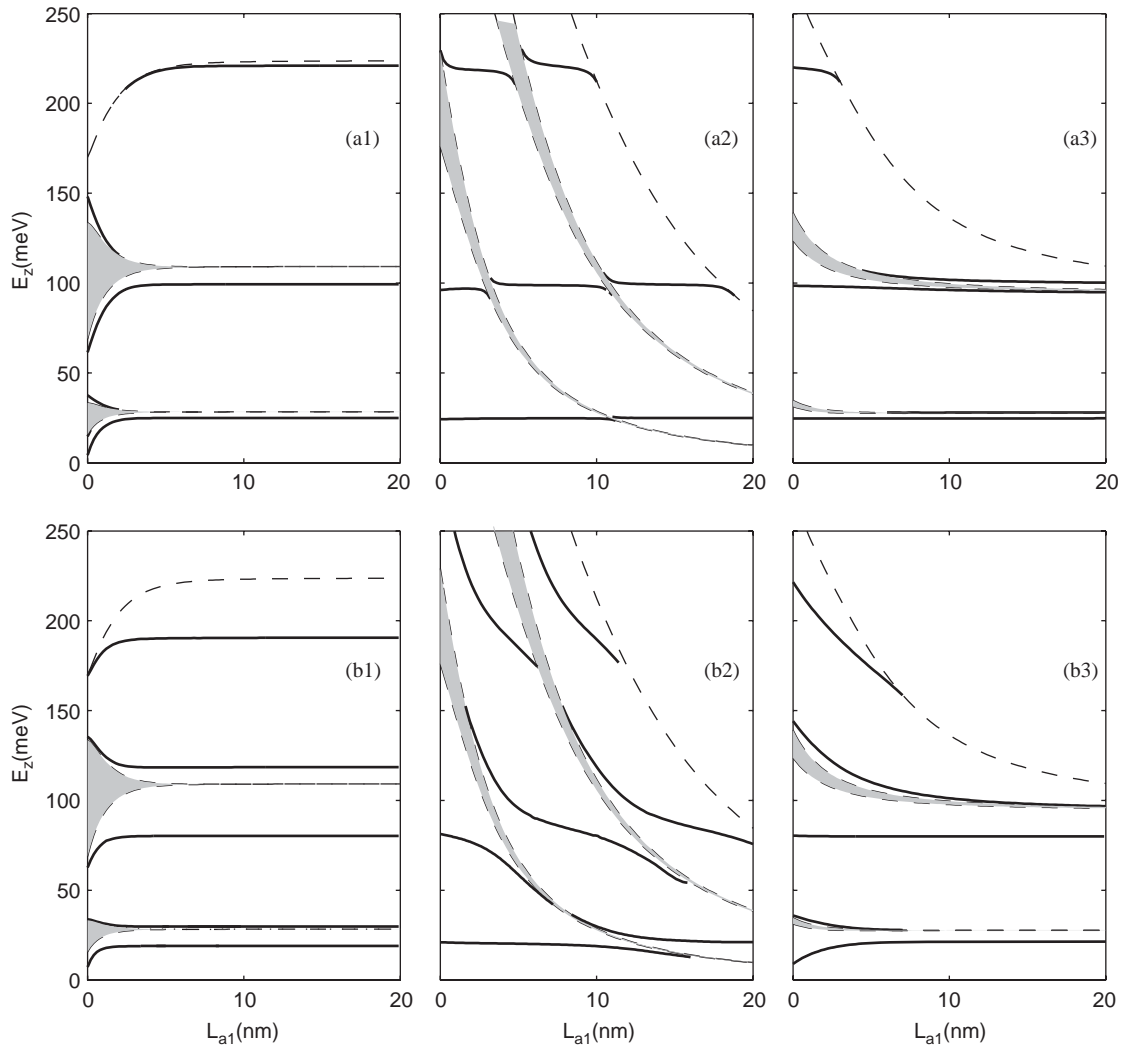


Fig. 7. Influence of different layer thickness variation on the localized electronic structure. For symmetric structure: (a1) L_{a1} variable, $L_{a2} = 10.0$ nm, $L_{a3} = 3.0$ nm; (a2) L_{a2} variable, $L_{a1} = 3.0$ nm, $L_{a3} = 3.0$ nm; (a3) L_{a3} variable, $L_{a1} = 3.0$ nm, $L_{a2} = 10.0$ nm. Here, $L_d = 12.0$ nm. Figs. 1(b), 2(b) and 3(b) for asymmetric structure, parameters are the same as for symmetric structure. Explanations for shaded areas and solid lines are the same as those in Fig. 2.

particular, we have numerically studied the coupling effect on the localized electronic states in a triple layer SL with a structural defect layer. A detailed comparison of localized electronic levels between symmetric and asymmetric structures is given. The results show some interesting physical effects: (1) the minibands are not influenced by the structural symmetry, while the localized states display different behaviors in both

symmetric and asymmetric structures; (2) a monotonic shifting towards the lower energy region of the minibands, minigaps and localized levels, narrowing of the minigaps and broadening of the minibands are found when increasing the transverse wave number k_{xy} , and the coupling effect is more obvious on the higher-lying minibands, minigaps and localized energy levels; (3) with the increase of the defect layer thickness L_d , the

localized states appear periodically in each minigap, and the branch number of the localized states increases with the index of the minigap for a given range of the thickness L_d ; (4) for symmetric structure, the parity of the localized states alternates between even and odd parity in each minigap.

Acknowledgements

This work was supported by the National Natural Science Foundation of China (Project Nos. 90403026).

References

- [1] V. Milanović, *Physica B* 121 (1983) 181.
- [2] G. Lenz, J. Salzman, *Appl. Phys. Lett.* 56 (1990) 871.
- [3] M. Stęślicka, R. Kucharczyk, M.L. Glasser, *Phys. Rev. B* 42 (1990) 1458.
- [4] H. Ohno, E.E. Mendez, J.A. Brum, J.M. Hong, F. Agulló-Rueda, L.L. Chang, L. Esaki, *Phys. Rev. Lett.* 64 (1990) 2555.
- [5] W.L. Bloss, *Phys. Rev. B* 44 (1991) 8035.
- [6] F. Capasso, C. Sirtori, J. Faist, D.L. Sivco, S.N.G. Chu, A.Y. Cho, *Nature* 358 (1992) 565.
- [7] D. Indjin, V. Milanović, Z. Ikonc, *Phys. Rev. B* 52 (1995) 16762.
- [8] E.H. El Boudouti, B. Djafari-Rouhani, A. Akjouj, L. Dobrzynski, R. Kucharczyk, M. Stęślicka, *Phys. Rev. B* 56 (1997) 9603.
- [9] R. Kucharczyk, M. Stęślicka, A. Akjouj, B. Djafari-Rouhani, L. Dobrzynski, E.H. El Boudouti, *Phys. Rev. B* 58 (1998) 4589.
- [10] M. Stęślicka, R. Kucharczyk, A. Kaczyński, *Vacuum* 63 (2001) 205.
- [11] A. Kaczynski, R. Kucharczyk, M. Stęślicka, *Physica E* 13 (2002) 59.
- [12] D.G. Sedrakyan, A.G. Sedrakyan, *Phys. Rev. B* 60 (1999) 10114.
- [13] Ke-Qiu Chen, Xue-Hua Wang, Ben-Yuan Gu, *Phys. Rev. B* 61 (2000) 12075;
Ke-Qiu Chen, Xue-Hua Wang, Ben-Yuan Gu, *Mod. Phys. Lett. B* 14 (2000) 571.
- [14] Xue-Hua Wang, Ke-Qiu Chen, Ben-Yuan Gu, *J. App. Phys.* 92 (2002) 5113.
- [15] Seiji Mizuno, *Phys. Rev. B* 65 (2002) 193302;
Seiji Mizuno, *Physica E* 17 (2003) 318.
- [16] Wen-Xia Li, Ke-Qiu Chen, W.H. Duan, J. Wu, B.L. Gu, *Phys. Lett. A* 308 (2003) 285.
- [17] N. Perrin, S. Tamura, *J. Phys.: Condens. Matter* 15 (2003) 693.
- [18] Ke-Qiu Chen, Xue-Hua Wang, Ben-Yuan Gu, *Phys. Rev. B* 62 (2000) 9919;
Ke-Qiu Chen, Xue-Hua Wang, Ben-Yuan Gu, *Phys. Rev. B* 65 (2002) 153305;
Ke-Qiu Chen, Wenhui Duan, Bing-Lin Gu, Ben-Yuan Gu, *Phys. Lett. A* 299 (2002) 634.
- [19] Ke-Qiu Chen, W.H. Duan, J. Wu, B.L. Gu, B. Ben-Yuan Gu, *J. Phys.: Condens. Matter* 14 (2002) 13761.
- [20] Xi-Li Zhang, Ben-Yuan Gu, Ke-Qiu Chen, *Phys. Lett. A* 316 (2003) 107.
- [21] Y.B. Li, M. Rocca, *J. Phys.: Condens. Matter* 5 (1993) 6597.
- [22] Xi-Li Zhang, Ben-Yuan Gu, Xue-Hua Wang, *J. Phys.: Condens. Matter* 16 (2004) 1075.
- [23] V.V. Paranjape, *Phys. Rev. B* 52 (1995) 10740.
- [24] Xue-Hua Wang, Ben-Yuan Gu, G.Z. Yang, *Phys. Rev. B* 55 (1997) 9340;
Xue-Hua Wang, Ben-Yuan Gu, G.Z. Yang, *Phys. Rev. B* 58 (1998) 4629.
- [25] J. Gong, S.L. Ban, X.X. Liang, *Int. J. Mod. Phys. B* 16 (2002) 4607.
- [26] Ke-Qiu Chen, Xue-Hua Wang, Ben-Yuan Gu, *Int. J. Mod. Phys. B* 14 (2000) 2587.
- [27] Wei-Qing Huang, Ke-Qiu Chen, Z. Shuai, L.L. Wang, W.Y. Hu, *Phys. Lett. A* 325 (2004) 70.